Check for updates

Lightweight and flexible MXene/CNF/silver composite membranes with a brick-like structure and high-performance electromagnetic-interference shielding†

Wei Xin, Guo-Qiang Xi, Wen-Tao Cao, Chang Ma, Tong Liu, Ming-Guo Ma [ID] *
and Jing Bian

With the increasing global electromagnetic pollution, it is more and more important to develop lightweight, flexible, and high electromagnetic shielding materials. Two-dimensional (2D) transition metal material MXenes have good conductivity and excellent electromagnetic shielding performance. Herein, a facile and effective method is reported to synthesize lightweight and flexible MXene/CNF/silver (MCS) composite membranes with a brick-like structure and high-performance electromagnetic interference shielding. MCS composite membranes have an electromagnetic shielding performance of ≈50.7 dB due to MXene self-reduction of silver nanoparticles and the brick-like structure, compared with that of MXene/CNF (MC) membranes (≈14.98 dB). In addition, the MCS composite membranes exhibit super-thin thickness (46 μm) and good tensile strength (up to 32.1 MPa), and their good mechanical properties are attributed to the addition of CNFs. Moreover, the MCS composite membranes show good electrical conductivity (588.2 S m^{-1}). Therefore, MCS composite membranes that are lightweight and flexible and have high electromagnetic shielding performance can replace other electromagnetic shielding materials and be used in aerospace, weapon equipment, and wearable smart materials.

Introduction

In the last few decades, the rapid development of various electronic communication technologies has brought great convenience and comfort to human life but also serious electromagnetic radiation.[1] As an invisible, intangible, and ubiquitous pollution factor, electromagnetic radiation has a negative impact on the environment.[2] It has been reported that electromagnetic waves can pass through the human skin into the human body to have a negative impact on people.[3–5] Recently, more attention has been paid to searching for suitable electromagnetic shielding materials to solve serious electromagnetic pollution.[6,7]

Metal materials (*e.g.*, Cu and Al) generally have high conductivity, which has been used as an effective way to weaken the electromagnetic radiation in the traditional sense.[8] Metallic materials also have excellent electrical conductivity and resistance to microwave penetration.[9] By effectively and uniformly

covering the material with a metal layer, good electrical conductivity can be obtained and applied to the electromagnetic shielding performance.[10,11] Silver is good conductive metal for electromagnetic shielding in non-woven fabrics applications.[12] For example, Wu *et al.* synthesized a 3.2 mm thick silver-plated sponge using dopamine as a reducing agent, exhibiting the SE$_{total}$ of 120.85 dB in the frequency range of 10–1500 MHz.[13] However, with the continuous promotion of portable intelligent electronic products, the characteristics of electromagnetic shielding materials are more lightweight and high electromagnetic shielding efficiency. In comparison with the traditional metal materials, the present carbon materials (such as carbon nanotubes,[14] graphene,[15] and reduced graphene oxide[16]) have the advantages of corrosion resistance, flexibility, high dielectric loss, and strong internal conductivity.[17,18]

In recent years, two-dimensional (2D) materials have been widely used in electromagnetic interference shielding.[19,20] With the continuous growth of the 2D material family, early transition metal carbides, nitrides, collectively named as MXenes.[21] MXenes (M$_{n+1}$X$_n$T$_x$, where n = 1, 2, 3, M means an early transition metal, X is C and/or N, and T means terminating group such as –F, –OH, –O)[22,23] are hydrophilic due to its many surface terminations.[24,25] MXenes are widely used in batteries,[26] supercapacitors,[27] photothermal conversion,[28]

Engineering Research Center of Forestry Biomass Materials and Bioenergy, Beijing Key Laboratory of Lignocellulosic Chemistry, College of Materials Science and Technology, Beijing Forestry University, Beijing 100083, PR China. E-mail: mg_ma@bjfu.edu.cn; Fax: +86-10-62336903; Tel: +86-10-62337250

sensors,[29] antibacterial activity,[30] catalysts,[31] and electromagnetic shielding.[32] With the increasing pollution of electromagnetic waves, MXene electromagnetic shielding materials are receiving tremendous attention and becoming increasingly important.[33] For example, Shahzad et al. reported a 45 μm thick $Ti_3C_2T_x$ film with electromagnetic interference (EMI) shielding effectiveness of 92 dB (>50 dB for a 2.5 μm film).[6] Weng et al. synthesized a semi-transparent LbL MXene-carbon nanotubes (CNTs) composite film with a maximum specific EMI shielding effectiveness of 58 187 dB cm^2 g^{-1}.[34] Wang et al. prepared a multifunction and water-resistant MXene-derived textiles with excellent EMI shielding efficiency of ≈90 dB at a thickness of 1.3 mm.[35] However, the mechanical strength of MXene is unsatisfactory, limiting its practical application in electromagnetic shielding.[36]

MXene has developed rapidly in recent years and has a promising potential applications.[35] Zhao et al. used MXene nanosheets as a flexible electrode in lithium–sulfur batteries, which had a capacity of 1029.7 mA h g^{-1} at 0.1C and maintains 946.7 mA h g^{-1} after 200 cycles with 91.9% retention.[26] Kim et al. prepared Ti_3C_2 with a very low limit of detection of 50–100 ppb for VOC gases at room temperature.[29] It was reported that the combination of MXene with a polymer could enhance the mechanical properties of MXene materials.[33] Compared with other polymer materials, cellulose nanofibers (CNFs) have good mechanical strength and biocompatibility, which can be widely used to improve the strength of materials.[37,38] In addition, cellulose can be used as a good electromagnetic shielding material by carbonizing cellulose after it is combined with metal materials and CNT materials.[39–41] Abdalla et al. reported light and flexible membranes with the R_L value of −46.60 dB was reached at 4.88 GHz frequency range.[39] In recent years, CNFs have been widely combined with conductive materials for supercapacitors,[42] batteries,[43] and conductive materials.[44] CNFs, as a one-dimensional linear material, can reduce the contact between MXene and its electrical conductivity on the basis of improving its mechanical strength. Meanwhile, CNFs can reduce the influence on the conductivity of 2D materials and metal particles. Cao et al. developed an ultrathin and flexible d-$Ti_3C_2T_x$/CNFs composite paper with the tensile strength (135.4 MPa) and electromagnetic shielding performance of 25.8 dB.[45]

Moreover, MXene also has the reducibility to reduce metal particles.[46–48] For example, Pandey et al. used MXene as a reducing agent to reduce silver nitrate solution to generate silver particles on the surface of MXene, which was applied to high-throughput and anti-pollution films.[46] However, the use of MXene reducibility in electromagnetic shielding has not been investigated.

In this study, we synthesized MXene-CNFs-silver (MCS) composite membranes using MXene reduced silver particles through the vacuum filtration method. The MCS composite membranes have good mechanical, electrical conductivity, and electromagnetic shielding, exhibiting electrical conductivity of 588.2 S m^{-1} and electromagnetic shielding properties of 50.7 dB. These membranes provide a new outstanding electromagnetic shielding material with a wide range of applications in aerospace, weapon equipment, and wearable smart fields.

Experimental

Materials

The never-dried bleached softwood kraft pulp obtained from DongHua Pulp Factory was applied to prepare cellulose nanofibers (CNFs) suspensions. MAX (Ti_3AlC_2) powders were purchased from Jilin 11 technology Co., Ltd. Hydrochloric acid (HCl), lithium fluoride (LiF), sodium bromide (NaBr), silver nitrate ($AgNO_3$), sodium hypochlorite (NaClO), and 2,2,6,6-tetramethylpiperidine-1-oxy (TEMPO) were purchased from Macklin. All the chemicals are a grade of analytical purity.

Preparation of delaminated $Ti_3C_2T_x$ nanosheets

The delaminated MXene was achieved by selectively etching Al species from MAX phase (Ti_3AlC_2) according to previous literature.[6] In this process, 1.0 g LiF and 20 mL of 9 M HCl were mixed in a Teflon vessel, and the mixture was stirred continuously. Then 1.0 g MAX (Ti_3AlC_2) added into it under magnetically stirred for 36 h at 35 °C. The multilayer MXene suspension was washed with deionized water to the pH value of ≈6, and the precipitates were obtained and collected. Finally, the MXene sediment was carried with deionized ions water for ultrasonic dispersal and centrifuged 4000 rpm to obtain MXene nanosheets for the synthesis of composite membranes.

Preparation of CNFs

The 1.0 g slurry plate was dispersed into a mixture solution of 0.0156 g TEMPO and 0.1028 g sodium bromide in 100 mL deionized water. Then 7.2 mL 10 wt% sodium hypochlorite solution was added to the mixture under stirring conditions. 0.1 mol L^{-1} NaOH solution was used to adjust the pH value around 10.5 until the pH value reaches stability. After the pH value was stabilized, dialysis was carried out in deionized water, and CNFs was obtained by high-pressure homogenization after dispersion.

Preparation of MXene-CNFs-silver (MCS) composite membranes

At room temperature, 15 mg MXene was removed with a pipette gun and placed in a beaker. 10 mL CNFs solution (1.0 wt%) was added to the beaker and stirred to form a stable mixed solution. In the stirring process, the 0.1 mol L^{-1} $AgNO_3$ solution was added drop by drop to form a uniform solution. Then the mixture solution was sonicated 10 min and stirring at room temperature for 12 h. The MCS composite membranes were obtained by the vacuum-assisted filtration method.

Characterization

Field emission scanning electron microscopy (FESEM) was used to observe the shapes of samples and energy spectrum element mapping (SU8010). The morphological representations were also carried out by a transmission electron microscope (TEM, JEM-1010, Japan). X-ray diffraction (XRD) was conducted with a Rigaku D/max 2550 V X-ray diffractometer. The surface chemistries of the composite membranes were characterized by

XPS with Kratos Analytical Ltd. Axis Ultra Scanning XPS Microprobe. TGA is a simultaneous heat treatment analyzer with a heating rate of 6 °C min^{-1} in flowing air (TA Q5000IR, USA). Fourier transform infrared spectra (FTIR) was performed by a Bruker, Tensor II IR spectrometer (FTIR-7600, Lambda Scientific, Australia). Conductivity was measured at room temperature by the standard four-probe method on the physical performance measurement system (ST2258C, Suzhou lattice electronics company). All samples were pre-cut to 2.0 × 2.0 mm and measured by a stainless steel ruler. The four-probe needle is close to the surface of the membrane, in which resistivity is obtained and conductivity is calculated. The mechanical properties of the MCS composite membranes were measured by a universal testing machine (Drick, China).

Electromagnetic shielding characterization

The electromagnetic shielding performance test is carried out by Agilent PNA-N5244A vector network analyzer, whose wavelength is 8.2–12.4 GHz. All samples were pre-cut to 22.9 × 10.2 mm size for testing. Place the sample in the sample rack and tighten it with a suitable screw to reduce the influence of glass on the experiment. S parameters (S_{11} and S_{21}) of each sample were recorded. The S parameter represents the transmission and reflection coefficient of the materials.[49] The EMI shielding effectiveness of MCS composite membranes is calculated as follows:[34]

$$SE_T = SE_A + SE_R + SE_M \tag{1}$$

SE_T, SE_R and SE_A can be expressed as:[34]

$$SE_T = 10 \log(1/|S_{21}|^2) \tag{2}$$

$$SE_R = 10 \log(1/1 - |S_{11}|^2) \tag{3}$$

$$SE_A = 10 \log(1 - |S_{11}|^2/|S_{21}|^2) \tag{4}$$

Generally speaking, the total shielding efficiency includes the contribution of absorption (SE_A), reflection (SE_R), and multiple reflections (SE_M). When $SE_T \geq 20$ dB, the SE_M can be negligible.

Specific shielding effectiveness (SSE) is often used to normalize the shielding performance of materials with different densities.[5] The eqn (5) was used to calculate the specific shielding effectiveness (SSE) and t means materials thickness.[34]

$$SSE/t = SE/(\text{thickness} \times \text{density}) = \text{dB cm}^2 \text{ g}^{-1} \tag{5}$$

Results and discussion

Preparation and characterization of MXene-CNFs-sliver (MCS) composite membranes

Fig. 1a illustrates the fabrication process of MXene-CNFs-sliver (MCS) composite membranes. HCl and LiF were used to selectively remove the Al layer from the Ti$_3$AlC$_2$ MAX phase and accordion-like MXene multi-layer structure was obtained. The
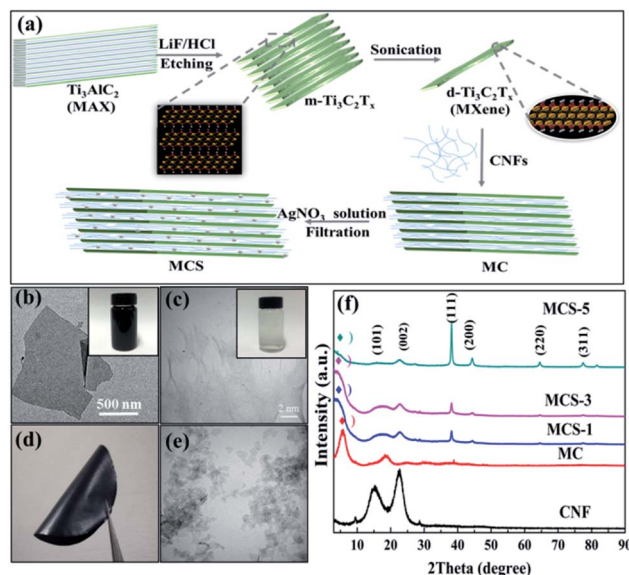

Fig. 1 (a) Illustration the preparation process of MCS composite membranes; (b and c) digital images and TEM images of (b) d-Ti$_3$C$_2$T$_x$ and (c) CNFs; (d) digital images of the MCS-3 composite membranes; (e) TEM image of m-Ti$_3$C$_2$T$_x$; (f) XRD patterns of the pure CNFs, MC, MCS-1, MCS-3, and MCS-5 composite membranes.

multilayer MXene was evenly dispersed in the suspension of MXene nanosheets by means of ultrasound to form a few layers of suspension. Then, the dispersions containing CNFs were added into the d-Ti$_3$C$_2$T$_x$ dispersions. The MCS composite membranes can be obtained by adding silver nitrate solution drop by drop to reduce silver particles in the stirring process. Fig. 1b shows the TEM image of a few layers of MXene sheet. The size of MXene sheet is between 1.0 μm and 1.5 μm. Meanwhile, CNFs are the aggregate structure of long fibers, and the length of the fibers is about 30–50 μm (Fig. 1c). MCS composite membranes were prepared by vacuum-assisted filtration method using MXene, CNF, and silver nitrate as suspensions (Fig. 1d). The TEM image of a multilayer MXene suspension was shown in Fig. 1e. XRD patterns indicated that MAX is selectively etched into accordion-like MXene from 9.6 to 6.6 degrees, and then ultrasonic into few-layer Ti$_3$C$_2$T$_x$ (Fig. 1f). In the previous literature, the transfer of the characteristic peaks implies the successful preparation of MXene nanosheets.[48]

The main peaks of CNFs belonged to the (101) and (002) planes, respectively, in which (101) plane corresponds to cellulose I, and then the crystal structure of cellulose I correspond to $2\theta = 22.6°$.[51] The MCS composite membranes displayed typical characteristic peaks of MXene and CNFs (Fig. 1f). The MCS composite membranes have different content of silver nitrate solution (MC: MXene-CNFs; MCS-1: MXene-CNFs-1 mL silver nitrate solution; MCS-3: MXene-CNFs-3 mL silver nitrate solution; MCS-5: MXene-CNFs-5 mL silver nitrate solution).

With the continuous addition of silver nitrate solution, the silver particles reduced by MXene increased. The characteristic peak of (002) plane in MXene changed from 6.6° to 5.0°,

indicating the appearance of silver nanoparticles due to the increase of interlayer spacing (Fig. S1†). The internal space of this change indicated that silver particles are evenly dispersed in multilayer MXene sheets. The scanning electron microscopy (SEM) image about Ti$_3$AlC$_2$ (MAX) is layered and bonded together before being etched (Fig. S2a†). Fig. S2b† shows the structure of the multi-layer MXene after etching. Because of the special accordion-like structure of MXene, it can be fully combined with other materials to prepare multi-functional polymer materials.

MXene has good dispersion in water by hydrogen bonding with other polar polymers due to its polar functional groups and terminal groups on its surface. MXene with good hydrophilicity is dispersed into homogeneous colloidal solution in water. Because the surface of MXene is negatively charged, it can be reduced with positively charged substances. XRD pattern displayed the characteristic peaks of (111), (200), (220), and (311) planes of silver (Fig. S3†).[46] The MXene peaks of (002) and (004) planes are also observed.[47] MXene reduces silver nitrate solution to produce silver nanoparticles. The opposite charges of MXene and silver ions provide a powerful driving force to contact each other and form a highly conductive MXene/silver composite. MXene has poor mechanical properties, meanwhile, CNFs have improved mechanical properties. Therefore, we propose to add CNFs to improve the mechanical properties of composites membranes.

Fig. 2 shows the top-view and cross-sectional SEM and TEM micrographs, representing the morphology of the MCS-1, MCS-3, and MCS-5 composite membranes. According to Fig. 2a, it can be seen that 1D CNFs and 2D lamellar MXene are uniformly combined, and the membranes obtained by the vacuum filtration have the smooth surface and tiny pores. With the continuous addition of silver nitrate solution, the number of silver particles can be clearly observed and gradually increased on the surface of the membranes. Fig. 2b shows that silver particles reduced by MXene were scattered inside and outside the membranes, with the MXene sheets wrapped by CNFs on the surface. With the increasing amount of silver nitrate solution, silver particles are densely and uniformly dispersed on the surface (Fig. 2c). Fig. 2d shows that a large number of silver

nanoparticles are evenly distributed on the surface of MCS-5 composite membranes and some of them are agglomerated. The cross-section of MCS-5 composite membranes displayed a brick-and-tile structure with silver nanoparticles in the MXene layers (Fig. 2e). This brick-and-tile structure not only provides internal reflection and absorption of electromagnetic wave but also further enhance its mechanical strength. In Fig. 2f, TEM image shows that silver nanoparticles are encapsulated by MXene and CNFs, and the size of silver nanoparticles is about 50 nm. The multilayer-Ti$_3$C$_2$T$_x$ are intertwined with CNFs, and there are silver nanoparticles wrapped in CNFs. Cross-sectional SEM images of the MCS composite membranes revealed their lamellar structure, and there are silver nanoparticles evenly distributed in each layer. By exploring the reduction of silver nanoparticles by MXene, the energy-dispersive X-ray spectroscopy (EDS) elemental mapping was applied to explore the distribution of various elements (Fig. S4†). With the increase of silver nitrate solution, the silver element is distributed randomly and its dispersion is increased. In the energy spectrum of MCS-5, the distribution of silver nanoparticles is more concentrated and dense, indicating the increasing amount of silver nanoparticles. The mass ratio of silver nanoparticles in MCS-1 is only 8.62 wt%. However, the mass ratio of silver nanoparticles in MCS-3 is increased to 17.67 wt%. Finally, the maximum value of silver nanoparticles in MCS-5 is 32.54 wt%. With the addition of the silver nitrate solution, silver nanoparticles are continuously obtained due to the reducibility of MXene.

The structure of chemical bonds on MXene surface chemical bonding, the self-reduction of silver, and the structure of MCS composite membranes can be detected by XPS analysis. The survey spectra of the MC composite membranes and MCS composites membranes indicate the presence of Ag components in composites membranes (Fig. 3a).[14] Furthermore, the spectrum of XPS showed the peak of Ag in MCS composite membranes with the increasing amount of silver nitrate solution. The intensity of the 3d Ag peak also increased as a function of the integrated silver nanoparticles. The contributions of Ti–C and C–O were reduced with respect to the Ag concentration in the composite matrix, but the contribution of C–C (or –CH$_2$ and –CH$_3$) was dominant. The peaks at ∼455.2 eV and ∼455.8 eV corresponded to Ti(II) and Ti(III), in addition to a minor Ti(IV) 2p peak located at 457 eV (Fig. 3b). With the continuous addition of silver nitrate solution, the peak values of Ti(IV) 2p$_{3/2}$ and Ti(IV) 2p$_{1/2}$ increased significantly, proving the silver nanoparticles on the surface of MXene through self-reduction. Ag$^+$ was immobilized on MXene surface by electrostatic adsorption to form MCS composites membranes (Fig. 3c). In addition, the difference of binding energy between two different doublets is 6 eV, indicating the appearance of silver nanoparticles in the MCS composite membranes. The 3d Ag spectra of the MCS composite membranes showed doublet peaks of the Ag 3d$_{5/2}$ and 3d$_{3/2}$ located at 368.1 eV and 374.1 eV, respectively (Fig. 3d). Fig. 3e shows a simple schematic diagram to illustrate the role of various materials in composite membranes so as to achieve a combination of performance optimization.
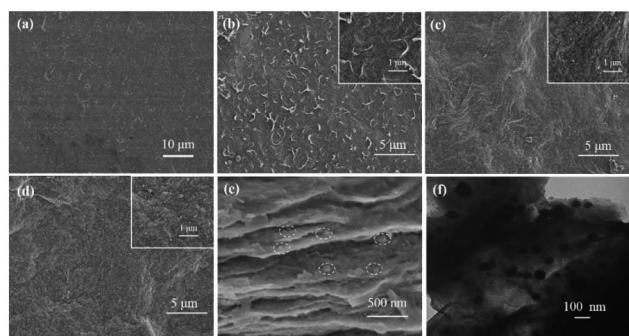

Fig. 2 SEM images of (a) the MC, (b) the MCS-1, (c) the MCS-3, (d) the MCS-5; (e) SEM image of the MCS-5 composite membranes, exhibiting a brick-like structure; (f) TEM micrograph of MCS-3 composite membranes.
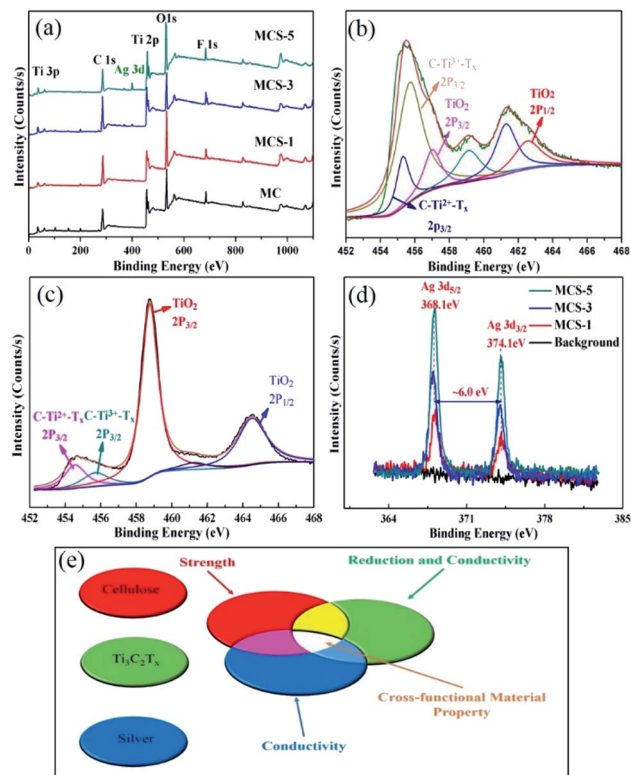
Fig. 3 (a) XPS survey spectra of the delaminated MC, MCS-1, MCS-3, and MCS-5; (b and c) XPS Ti 2p core level spectra of (b) MXene and (c) MCS-3; (d) the high-resolution XPS spectra of Ag 3d for the MCS-3; (e) illustrate how to design cross-functional materials by controlling the arrangement and assembly of nanostructures of MXenes, CNFs, and silver nanoparticles.

Fourier transform infrared (FTIR) spectra of pure CNFs, pure MXene, and MCS-3 composite membranes are shown in Fig. S5.† MXene ($Ti_3C_2T_x$) has one typical peak at 563 cm^{-1}, corresponding to the surface terminal group of C–F. When CNFs is combined with MXene, the absorption peak of CNFs locate at 3439 cm^{-1}, corresponding to the –OH stretching vibration peak.[9] The –OH bending is observed at 1622 cm^{-1}. CH_2 bending vibration peak is located at 1396 cm^{-1}.[13] The typical stretching peaks of C–O bond are observed at 1068 cm^{-1} corresponding to the characteristic peaks of MXene.[45] These infrared data are sufficient to prove the linked CNFs and MXene.

Electrical conductivity, mechanical property, and electromagnetic shielding performance of MXene-CNFs-sliver (MCS) composite membranes

Conductivity is an important factor for the performance of electromagnetic shielding.[34] MCS-1 composite membranes had an electrical conductivity of 418.4 S m^{-1} (Fig. S6†), which was more than 43 times that of the MC composite film (9.69 S m^{-1}).[45] The conductivity of MCS-3 composite membranes reached to 588.2 S m^{-1}, indicating the increased conductivity significantly. The addition of silver nanoparticles on MXene is beneficial to the electrical conductivity of composites.[8] The SEM

image shows that the conductivity increases, then decreases with the increasing amount of silver nanoparticles (Fig. S6†). The conductivity of MCS-5 composite membranes decreases to 273.9 S m^{-1}. CNFs are an insulating material. With the increasing amount of silver nanoparticles reduced by MXene, silver nanoparticles agglomerated to a certain extent, and then coated by 1D CNFs fibers, increasing the impedance of the material. MXene is reducible to some extent, and a certain amount of silver nanoparticles are reduced to make the conductivity and electromagnetic shielding properties of the materials increase continuously. However, with the reduction of silver nanoparticles, MXene is oxidized to other material with low conductivity. Although the production of silver nanoparticles is increased, the conductivity and electromagnetic shielding performance of composites decrease. Therefore, one can conclude that the conductivity of silver nanoparticles will be increased to a certain extent, but the conductivity of composites will be decreased by excessive reduction.

The absorption characteristics of electromagnetic wave are mainly related to relative permeability, relative dielectric constant, skin depth δ and the microstructure of the absorber materials.[49] The absorption enhancement shielding of materials is mainly attributed to the interaction between electric dipoles or magnetic dipoles and electromagnetic waves.[3] Materials need to move charged carriers (electrons or holes) in order to interact with the incident electromagnetic waves, so as to achieve electromagnetic shielding reflection.[50] Kumar *et al.* investigated the electromagnetic shielding properties like complex permittivity, complex permeability, *S*-parameters, and various shielding effectiveness for the MXene-PANI composite (50% wt) in the microwave frequency range (8.2–12.2 GHz).[52] They found that the real part and imaginary part of the relative complex permittivity values are high due to the high conductivity of MXene.[52,53] In addition, magnetic loss have important significance in microwave absorption.[54] Under the action of alternating electromagnetic field, both the electromagnetic dissipation ability and the existence of active polar groups can be used to illustrate the high conductivity of the composite material.[52] Multiple internal reflections are caused by scattering centers, including interface or defect points in shielding materials.[32] The dielectric constant of MAX increases remarkably after the removal of the aluminum layer.[50] This is due to the characteristics determined by the surface groups and the high conductivity, which play an important role in the electromagnetic shielding performance of the composite. To some extent, conductivity affects electromagnetic shielding.[19] As for the distribution of conductive fillers in the frame structure, it is widely acknowledged that the establishment of the conductive network is very important to the conductive performance, so it has a significant impact on the shielding performance of EMI.[8] The traditional metal materials have good electromagnetic shielding performance, but they are easily corroded and have high density, which limits their practical applications.[9,13] Carbon-based materials generally have high electromagnetic shielding energy and low density, such as multi-layer carbon nanotubes,[14] reduced graphene oxide,[16] and so on. In order to make full use of the inherent electromagnetic shielding ability

of MXene, the distribution rule of beneficial fillers in the frame structure is creatively proposed, instead of simply improving the mass ratio of nano-fillers. All the electromagnetic shielding performance of MCS composite membranes with different content of silver nitrate solution (MC: MXene-CNFs; MCS-1: MXene-CNFs-1 mL silver nitrate solution; MCS-3: MXene-CNFs-3 mL silver nitrate solution; MCS-5: MXene-CNFs-5 mL silver nitrate solution) exceed 20 dB, as shown in Fig. 4a. By combining CNF with MXene, with the increasing of MXene, it is beneficial to the charge movement.[45] To some extent, silver nanoparticles produced by MXene reduction can improve the conductivity and electromagnetic shielding properties of materials. In addition, silver nanoparticles create more circuits and provide more free electrons.[13] The interfacial affinity between MXene and silver nanoparticles increases the number of conductive pathways for electron transfer.[8] All these factors can improve the conductivity of the composites and the electromagnetic interference intensity. The electromagnetic shielding performance of MC membranes was only 14.89 dB. The combination of MXene and CNFs not only improves its mechanical strength but also provides more internal microwave

diffusion interfaces.[45] Because of self-reduction of MXene, the reduction of hydroxyl groups on MXene surface and the formation of the multilayered structure increases the conductivity of electrons, and the dielectric constant increases continuously, having a positive effect on the conduction loss.[50] After the addition of silver nanoparticles, the electromagnetic shielding performance of MCS composite membranes was improved dramatically. An electromagnetic shielding performance of 28.01 dB was obtained for the MCS-1 composite membranes and 50.70 dB for MCS-3 composite membranes, meeting the requirements of commercial electromagnetic shielding. MCS-5 composite membranes displayed the electromagnetic shielding performance of 27.51 dB, which was similar to that of MCS-1 composite membranes. The electromagnetic shielding performance of the above three samples is much higher than the standard for commercial applications. All the absorption, reflection, and multi-layer internal reflection are the main links of electromagnetic shielding.[16] The multilayer internal reflection is extremely small and negligible when SE_{total} is greater than 20 dB.[5] One can observe that the value of absorption is higher than that of reflection (Fig. 4b), which plays a major role in electromagnetic shielding. In the literature, the related polymer nanocomposites reported the similar results, among which the SE_R value increased slightly with the increase of conductivity.[14] Similar to the conductivity performance, the electromagnetic shielding performance presents a similar continuous improvement. When silver nanoparticles are encapsulated by CNFs agglomeration, the electromagnetic shielding performance decreases.[45] The SE_{Total}, SE_A, and SE_R of the MCS-3 composite membranes are ~50.7 dB, ~22.0 dB, and ~27.7 dB at 12.4 GHz, respectively. So far, in comparison with the electromagnetic shielding performance in the literature, the MCS composite membranes have very low thickness and excellent electromagnetic shielding performance (Fig. 4c and Table S1†). Among them, electromagnetic waves in layered MCS composite membranes can be reflected internally many times, leading to the continuous absorption and energy loss of electromagnetic waves. The effect of the addition of silver nanoparticles on SSE/t of MCS composite membranes is very significant in the X-band region (Fig. 4d). Fig. 4e illustrates vividly how the electromagnetic shielding performance attenuates electromagnetic waves and the effects of absorption, reflection, and internal refraction. The electromagnetic shielding performance of MCS composite membranes can be effectively improved by the increasing content of silver nanoparticles. In addition, MCS-3 composite membranes can shield about 99.9% of electromagnetic waves at 8.2 GHz.

There is a certain Tyndal effect in the mixed solution of MCS composite membranes (Fig. S8†). In this paper, the mechanical properties were significantly improved, from the initial tensile strength of 1.80 ± 0.16 MPa of MXene to 13.90 ± 0.39 MPa for the MCS-1 composite membranes, and then through further upgrading to the tensile strength of 32.10 ± 3.80 MPa for MCS-3 composite membranes. The tensile strength of MCS-5 composite membranes can reach 34.20 ± 7.20 MPa, which is higher than that of pure MXene (Fig. 5a and Table S2†).
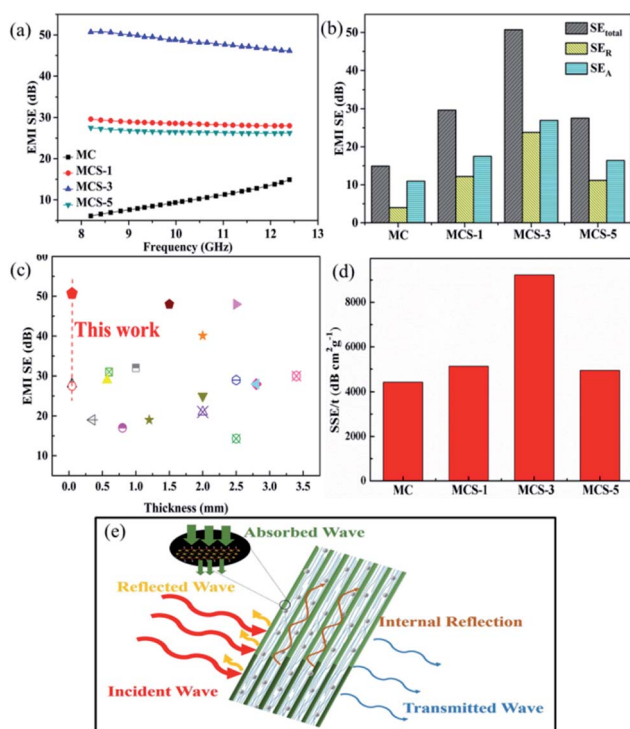

Fig. 4 (a) The effect of silver nitrate solution addition on EMI SE of different MCS composite membranes with different thickness in the X-band region; (b) comparison of total EMI shielding effectiveness (SE_Total), microwave absorption (SE_A), and microwave reflection (SE_R) at a frequency of 12.4 GHz of the MCS composite membranes with different silver nitrate solution; (c) comparison of the specific EMI shielding effectiveness of different materials (i.e. carbon-based, MXene-based, CNT-based, and MCS composite membranes); (d) effect of silver nitrate content on the SSE/t of the MCS composite membranes with different silver nitrate contents in the X-band region; (e) proposed EMI shielding mechanism of the MCS composite membranes.
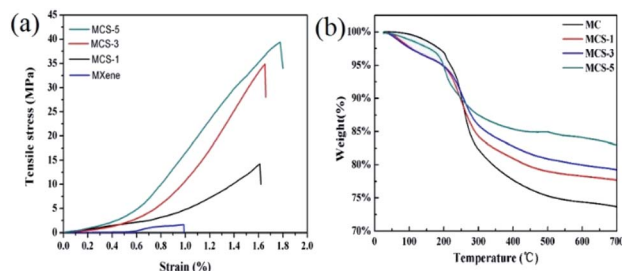
Fig. 5 (a) Tensile strengths and (b) TG curves of the MCS composite membranes with different silver nitrate solution.

The mechanical properties of MCS composite membranes far exceed the mechanical strength of pure MXene membranes, indicating that there is a strong interaction between the layered structure of bricks and tiles composed of 0D silver nanoparticles, 1D CNFs fibers, and 2D MXene nanosheets (Fig. S9†).[55] 2D MXene nanosheets have a large number of terminal functional groups (e.g., F, O, and OH) and 1D CNFs fibers also have active hydroxyl groups. The experimental results show that the mechanical strength can be improved by adding CNFs, and the mechanical properties can be further improved to a certain extent by combining the hydrogen bonding and van der Waals force between layers produced by adding 0D silver nanoparticles. In the self-assembled layered structure formed by the vacuum filtration method, there are some voids in the tight bonding between MXene and CNFs. The silver nanoparticles in the voids are the uniform distribution and close to the layered structure. The formation of silver nanoparticles increases the interface between layers, especially the intertwining of silver nanoparticles with MXene and CNFs, which further increases the strength. The increase of silver nanoparticles can slightly improve the mechanical properties of the material, mainly due to the increase of physical winding. The winding of MXene and silver nanoparticles by CNFs is more disorderly, and the interaction between CNFs fibers increases. The hydrogen bond between MXene and CNFs was first destroyed during the stretching process. As the stretching force increased, the winding between CNFs and silver nanoparticles and MXene continued to break. At the same time, silver nanoparticles can provide a series of friction energy loss between MXene nanosheets and CNFs fibers to further weaken the sliding effect of MXene, which can toughen the material until cracks occur. Because CNFs have very high tensile strength, the interaction between CNFs molecular chains to avoid further tensile fracture can consume more energy in the process of drawing.[56,57] Moreover, the winding of CNFs and silver nanoparticles and the uniform distribution of silver nanoparticles in the MXene sheets constructed by silver nanoparticles and MC can increase the friction loss energy, and the anisotropic network structure constructed by CNFs also plays an important role in fracture.[58] The study of fracture morphology and mechanism proves that the composite membranes are a special layered structure composed of "Brick-like structure" (Video S1, ESI†).[59] Through this combination, certain strength and

toughness can be improved. In the framework of the composite, CNFs can be used as cement, mainly connecting the corresponding MXene and silver nanoparticles for stress transfer and dispersion. Silver nanoparticles increase their strength and can cause friction energy loss during fracture. The synergistic effect of 2D MXene, 1D CNFs, and 0D silver nanoparticles on toughening can further enhance its strength and toughness. In Fig. 5b and Table S3,† the thermal stability of composite membranes was determined by thermogravimetric analysis. At the initial stage below 100 °C, the water adsorbed on its surface membranes is gradually evaporated. With the increase of temperature, the oxygen-containing functional groups on the surface of CNFs and the water on MXene nanosheets gradually decompose, and the main quality deterioration factor is the carbonization of CNFs, so the quality of membranes decreases sharply. The thermal stability of the MCS composite membranes can be improved by adding silver nanoparticles. Thermogravimetric loss of MCS-5 composite membranes is only 16%, while that of the similar MC membrane is about 26%.

Conclusions

In summary, we prepared the lightweight and flexible MXene/CNFs/silver composite membranes by the vacuum filtration method. The composite membranes have brick-like layered nanostructures, good conductivity, improve mechanical properties, and super high electromagnetic shielding performance. MCS-5 composite membranes have the mechanical properties of 34.2 MPa, compared with that of pure MXene membranes (1.78 MPa). MCS-3 composite membranes displayed the electromagnetic shielding properties of 50.7 dB, in comparison with that of MC membranes (14.89 dB). In addition, MCS-3 composite membranes exhibit excellent electrical conductivity (588.2 S m^{-1}). Both the brick-like structure and silver nanoparticles provide more ways for microwave absorption and scattering. We proposed a self-reducing structure of 2D MXene nanosheets to reduce 0D silver nanoparticles, and a special structure of brick-like layered nanostructures constructed by 1D CNFs fibers to be applied in the field of electromagnetic shielding and self-assembly. This method utilizes the MXene's good electrical conductivity and good reducibility to apply to electromagnetic shielding performance, and combines with its brick-like structure constructed by CNFs fibers, will expand the application scope of MXene's electromagnetic shielding materials. Therefore, the lightweight and flexible MXene/CNFs/silver composite membranes with excellent EMI shielding performance will be highly promising in aerospace, applications for defense, and smart and flexible electronics.

Conflicts of interest

There are no conflicts to declare.

Acknowledgements

References

1 M. Cao, X. Wang, W. Cao, X. Fang, B. Wen and J. Yuan, *Small*, 2018, **14**, 1800987.

2 Q. Zhang, Q. Liang, Z. Zhang, Z. Kang, Q. Liao, Y. Ding, M. Ma, F. Gao, X. Zhao and Y. Zhang, *Adv. Funct. Mater.*, 2017, **28**, 1703801.

3 D. D. L. Chung, *Carbon*, 2001, **39**, 279–285.

4 N. Yousefi, X. Sun, X. Lin, X. Shen, J. Jia, B. Zhang, B. Tang, M. Chan and J. K. Kim, *Adv. Mater.*, 2014, **26**, 5480–5487.

5 J. Liu, H. B. Zhang, R. Sun, Y. Liu, Z. Liu, A. Zhou and Z. Yu, *Adv. Mater.*, 2017, **29**, 1702367.

6 F. Shahzad, M. Alhabeb, C. B. Hatter, B. Anasori, S. M. Hong, C. M. Koo and Y. Gogotsi, *Science*, 2016, **353**, 1137–1140.

7 X. Li, X. Yin, S. Liang, M. Li, L. Cheng and L. Zhang, *Carbon*, 2019, **146**, 210–217.

8 Y. Chen, Y. Li, M. Yip and N. Tai, *Compos. Sci. Technol.*, 2013, **80**, 80–86.

9 T. W. Lee, S. E. Lee and Y. G. Jeong, *ACS Appl. Mater. Interfaces*, 2016, **8**, 13123–13132.

10 H. Wang, C. Ji, C. Zhang, Y. Zhang, Z. Zhang, Z. Lu, J. Tan and L. J. Guo, *ACS Appl. Mater. Interfaces*, 2019, **11**, 11782–11791.

11 A. Ameli, P. U. Jung and C. B. Park, *Carbon*, 2013, **60**, 379–391.

12 Y. J. Tan, J. Li, Y. Gao, J. Li, S. Guo and M. Wang, *Appl. Surf. Sci.*, 2018, **458**, 236–244.

13 L. P. Wu, Y. Z. Li, B. J. Wang, Z. P. Mao, H. Xu, Y. Zhong, L. Zhang and X. F. Sui, *Mater. Des.*, 2018, **159**, 47–56.

14 Y. Zhan, M. Oliviero, J. Wang, A. Sorrentino, G. G. Buonocore, L. Sorrentino, M. Lavorgna, H. S. Xia and S. Iannace, *Nanoscale*, 2019, **11**, 1011–1020.

15 C. Xiang, R. Guo, S. Lin, S. Jiang, J. Lan, C. Wang, C. Cui, H. Xiao and Y. Zhang, *Chem. Eng. J.*, 2019, **360**, 1158–1166.

16 B. Wen, M. Cao, M. Lu, W. Cao, H. Shi, J. Liu, X. Wang, H. Jin, X. Fang, W. Wang and J. Yuan, *Adv. Mater.*, 2014, **26**, 3484–3489.

17 H. Abbasi, M. Antunes and J. I. Velasco, *Prog. Mater. Sci.*, 2019, **103**, 319–373.

18 S. Zhu, C. Xing, F. Wu, X. Zuo, Y. Zhang, C. Yu, M. Chen, W. Li, Q. Li and L. Liu, *Carbon*, 2019, **145**, 259–265.

19 M. S. Cao, Y. Z. Cai, P. He, J. C. Shu, W. Q. Cao and J. Yuan, *Chem. Eng. J.*, 2018, **359**, 1265–1302.

20 X. Ye, J. Hu, B. Li, M. Hong and Y. Zhang, *Chem. Eng. J.*, 2019, **361**, 1110–1120.

21 V. M. H. Ng, H. Huang, K. Zhou, P. S. Lee, W. Que, J. Z. Xu and L. B. Kong, *J. Mater. Chem. A*, 2017, **5**, 3039–3068.

22 M. R. Lukatskaya, O. Mashtalir, C. E. Ren, Y. Dall'Agnese, P. Rozier, P. L. Taberna, M. Naguib, P. Simon, M. W. Barsoum and Y. Gogotsi, *Science*, 2013, **341**, 1502–1505.

23 M. Naguib, V. N. Mochalin, M. W. Barsoum and Y. Gogotsi, *Adv. Mater.*, 2014, **26**, 992–1005.

24 J. Zhao, Y. Yang, C. Yang, Y. Tian, Y. Han, J. Liu, X. Yin and W. Que, *J. Mater. Chem. A*, 2018, **6**, 16196–16204.

25 W. T. Cao, W. Feng, Y. Y. Jiang, M. Chang, Z. F. Zhou, M. G. Ma, Y. Chen and F. Chen, *Mater. Horiz.*, 2019, **6**, 1057–1065.

26 Q. Zhao, Q. Zhu, J. Miao, P. Zhang and B. Xu, *Nanoscale*, 2019, **11**, 8442–8448.

27 Y. Tian, W. Que, Y. Luo, C. Yang, X. Yin and L. B. Kong, *J. Mater. Chem. A*, 2019, **7**, 5416–5425.

28 H. Lin, X. Wang, L. Yu, Y. Chen and J. Shi, *Nano Lett.*, 2016, **17**, 384–391.

29 S. J. Kim, H. J. Koh, C. E. Ren, O. Kwon, K. Maleski, S. Y. Cho, B. Anasori, C. K. Kim, Y. K. Choi, J. Kim, H. T. Jung and Y. Gogotsi, *ACS Nano*, 2018, **12**, 986–993.

30 K. Rasool, M. Helal, A. Ali, C. E. Ren, Y. Gogotsi and K. A. Mahmoud, *ACS Nano*, 2016, **10**, 3674–3684.

31 J. Ran, G. Gao, F. T. Li, T. Y. Ma, A. Du and S. Z. Qiao, *Nat. Commun.*, 2017, **8**, 13907.

32 W. Cao, C. Ma, S. Tan, M. G. Ma, P. B. Wan and F. Chen, *Nano-Micro Lett.*, 2019, **11**, 72.

33 R. Sun, H. B. Zhang, J. Liu, X. Xie, R. Yang, Y. Li, S. Hong and Z. Z. Yu, *Adv. Funct. Mater.*, 2017, **27**, 1702807.

34 G. M. Weng, J. Li, M. Alhabeb, C. Karpovich, H. Wang, J. Lipton, K. Maleski, J. Kong, E. Shaulsky, M. Elimelech, A. D. Taylor and Y. Gogotsi, *Adv. Funct. Mater.*, 2018, **28**, 1803360.

35 Q. W. Wang, H. B. Zhang, J. Liu, S. Zhao, X. Xie, L. Liu, R. Yang, N. Koratkar and Z. Z. Yu, *Adv. Funct. Mater.*, 2019, **29**, 1806819.

36 Z. Ling, C. E. Ren, M. Q. Zhao, J. Yang, J. M. Giammarco, J. Qiu, M. W. Barsoum and Y. Gogotsi, *Proc. Natl. Acad. Sci. U. S. A.*, 2014, **111**, 16676–16681.

37 R. J. Moon, A. Martini, J. Nairn, J. Simonsen and J. Youngblood, *Chem. Soc. Rev.*, 2019, **40**, 3941–3994.

38 M. Jonoobi, J. Harun, A. P. Mathew and K. Oksman, *Compos. Sci. Technol.*, 2010, **70**, 1742–1747.

39 I. Abdalla, A. Salim, M. M. Zhu, J. Y. Yu, Z. L. Li and B. Ding, *ACS Appl. Mater. Interfaces*, 2018, **10**, 44561–44569.

40 I. Abdalla, J. L. Shen, J. Y. Yu, Z. L. Li and B. Ding, *Sci. Rep.*, 2018, **8**, 12402.

41 I. Abdalla, J. Y. Yu, Z. L. Li and B. Ding, *Composites, Part B*, 2018, **155**, 397–404.

42 K. Gao, Z. Shao, J. Li, X. Wang, X. Peng, W. Wang and F. Wang, *J. Mater. Chem. A*, 2013, **1**, 63–67.

43 S. Cao, X. Feng, Y. Song, X. Xue, H. Liu, M. Miao, J. Fang and L. Shi, *ACS Appl. Mater. Interfaces*, 2015, **7**, 10695–10701.

44 H. Koga, M. Nogi, N. Komoda, T. T. Nge, T. Sugahara and K. Suganuma, *NPG Asia Mater.*, 2014, **6**, e93.

45 W. T. Cao, F. F. Chen, Y. J. Zhu, Y. G. Zhang, Y. Y. Jiang, M. G. Ma and F. Chen, *ACS Nano*, 2018, **12**, 4583–4593.

46 R. P. Pandey, K. Rasool, V. E. Madhavan, B. Aïssa, Y. Gogotsi and K. A. Mahmoud, *J. Mater. Chem. A*, 2018, **6**, 3522–3533.

47 Y. Jiang, X. Zhang, L. Pei, S. Yue, L. Ma, L. Zhou, Z. Huang, Y. He and J. Gao, *Chem. Eng. J.*, 2018, **339**, 547–556.

48 E. Satheeshkumar, T. Makaryan, A. Melikyan, H. Minassian, Y. Gogotsi and M. Yoshimura, *Sci. Rep.*, 2016, **6**, 32049.

49 Y. K. Hong, C. Y. Lee, C. K. Jeong, D. E. Lee, K. Kim and J. Joo, *Rev. Sci. Instrum.*, 2003, **74**, 1098–1102.

50 N. Li, Y. Huang, F. Du, X. He, X. Lin, H. Gao, Y. Ma, F. Li, Y. Chen and P. C. Eklund, *Nano Lett.*, 2006, **6**, 1141–1145.

51 M. S. Cao, W. L. Song, Z. L. Hou, B. Wen and J. Yuan, *Carbon*, 2010, **48**, 788–796.

52 S. Kumar, P. Kumar, N. Singh and V. Verma, *J. Magn. Magn. Mater.*, 2019, **488**, 165364.

53 M. Mo, L. Zhang and G. Wang, *Nanostruct. Mater.*, 1995, **6**, 823–826.

54 B. Lu, X. L. Dong, H. Huang, X. F. Zhang, X. G. Zhu and J. P. Lei, *J. Magn. Magn. Mater.*, 2008, **320**, 1106–1111.

55 M. Han, X. Yin, H. Wu, Z. Hou, C. Song, X. Li, L. Zhang and L. Cheng, *ACS Appl. Mater. Interfaces*, 2016, **8**, 21011–21019.

56 Y. Zhang, L. Li, L. Zhang, S. Ge, M. Yan and J. Yu, *Nano Energy*, 2017, **31**, 174–182.

57 H. Xu, X. Yin, X. Li, M. Li, S. Liang, L. Zhang and L. Cheng, *ACS Appl. Mater. Interfaces*, 2019, **11**, 10198–10207.

58 Z. Tang, N. A. Kotov, S. Magonov and B. Ozturk, *Nat. Mater.*, 2003, **2**, 413.

59 R. Xiong, K. Hu, A. M. Grant, R. Ma, W. Xu, C. Lu, X. Zhang and V. V. Tsukruk, *Adv. Mater.*, 2016, **28**, 1501–1509.